Supplementary Information

Ionic liquid gel microspheres as an emerging platform for constructing liquid compartment microreactors

Dongqing He [a], Dezhou Cao [a, b], Chuxuan Ben [a], Yalin Lan [a, c], He Zhang [a], Meijiao Jiang [a], Shuyao Wu [a], Yu Zhang [a], Qing Bo Meng [a, *] and Xi-Ming Song [a, *]

[a] *Liaoning Key Laboratory for Green Synthesis and Preparative Chemistry of Advanced Materials, College of Chemistry, Liaoning University, Shenyang 110036, China*

[b] *School of Materials Science and Engineering, Harbin Institute of Technology (Shenzhen), Shenzhen, Guangdong 518055, China*

[c] *Analysis Center, Shenyang University of Chemical Technology, Shenyang 110141, China*

** Corresponding authors. E-mail: mengqb@lnu.edu.cn (Qing Bo Meng); songlab@lnu.edu.cn (Xi-Ming Song)*

Supplementary Methods

Materials

1-butyl-3-methylimidazolium hexafluorophosphate ([BMIM]PF_6, 99%), ciprofloxacin (98%) and poly(vinyl alcohol) 1799 (PVA, GR) were purchased from Shanghai Macklin Biochemical Co., Ltd. Methyl methacrylate (MMA, CP), potassium persulfate (KPS, AR), polyvinyl pyrrolidone (PVP, K30, GR), ethylene glycol (AR), absolute methanol (AR) and borax (AR) were purchased from Sinopharm Chemical Reagent Co., Ltd. Bismuth nitrate pentahydrate ($Bi(NO_3)_3 \cdot 5H_2O$, 99%), potassium bromide (KBr, 99%), rhodamine B (RhB, 99%), coumarin 6 (98%) and fluorescein sodium (AR) were purchased from Shanghai Aladdin Biochemical Technology Co., Ltd. All of the reagents and solvents were used as received without further purification.

Preparation of bulk IL-gels

Firstly, a certain mass ratio of MMA and [BIMM]PF_6 were added into a vial containing azobisisobutyronitrile (AIBN) with a AIBN/MMA mass ratio of 0.5%, and then the system was uniformly mixed under ultrasonication. Finally, the bulk IL-gels were obtained by placing vials in an oven at 80 °C for 20 minutes and then 60 °C for 12 h.

Preparation of PMMA

Firstly, 0.08 g of PVP was dissolved in 70 mL of deionized water as the aqueous phase, 10 g of MMA as oil phase monomer, and the initiator solution was prepared by dissolving 0.1 g of KPS in 10 mL of deionized water under ultrasonication. Next, the aqueous phase and the oil phase were charged into a three-necked flask and continuously stirred at 300 rpm for 30 min to form stable emulsion. Then the system was heated to 80 ºC, and the initiator solution was added to the flask in three divided batches at the interval of 1 h. After all the initiator solution was added to the system, the reaction was conducted for 4 h under this condition, and then further elevated to 100 °C and maintained for 1 h. Finally, the PMMA was obtained after centrifugation and washing with distilled water for several times, followed by freeze-drying at −40 °C under vacuum for 12 h.

Preparation of PILs microspheres

PILs microspheres were prepared by dispersion polymerization. Briefly, 0.2 g of 1-butyl-3-vinylimidazolium hexafluorophosphate ([BVIM]PF_6), 0.1 g of PVP and 0.01 g of AIBN were added into a round bottom flask containing 20 mL of absolute ethanol, then polymerization was performed at 80 °C for 10 h. The product was isolated by centrifugation and washing with distilled water for several times, followed by freeze-drying at −40 °C under vacuum for 12 h.

Preparation of BiOBr microspheres

Briefly, 1.4 mmol of $Bi(NO_3)_3\cdot 5H_2O$, 1.4 mmol of KBr and 0.02 g of PVP were added slowly into 30 mL of ethylene glycol. The mixture was ultrasonically treated for 1 h, and then magnetically stirred for 2 h. Subsequently, the mixture was transferred into a 50 mL Teflon-lined stainless steel autoclave. The autoclave was then sealed and maintained at 150 °C for 12 h. After cooling down to room temperature, the BiOBr microspheres were obtained after centrifugation and washing with distilled water for several times, followed by freeze-drying at −40 °C under vacuum for 12 h.

Preparation of BiOBr-[BMIM]PF_6

Briefly, 1.4 mmol of $Bi(NO_3)_3\cdot 5H_2O$, 1.4 mmol of KBr, 0.02 g of PVP and 0.1 g of [BMIM]PF_6 were added slowly into 30 mL of ethylene glycol. The mixture was ultrasonically treated for 1 h, and then magnetically stirred for 2 h. Subsequently, the mixture was transferred into a 50 mL Teflon-lined stainless steel autoclave. The autoclave was then sealed and maintained at 150 °C for 12 h. After cooling down to room temperature, the BiOBr-[BMIM]PF_6 were obtained after centrifugation and washing with distilled water for several times, followed by freeze-drying at −40 °C under vacuum for 12 h.

Preparation of BiOBr@PMMA

Briefly, 1.4 mmol of $Bi(NO_3)_3 \cdot 5H_2O$, 1.4 mmol of KBr, 0.02 g of PVP and 0.1 g of PMMA were added slowly into 30 mL of ethylene glycol. The mixture was ultrasonically treated for 1 h, and then magnetically stirred for 2h. Subsequently, the mixture was transferred into a 50 mL Teflon-lined stainless steel autoclave. The autoclave was then sealed and maintained at 150 °C for 12 h. After cooling down to room temperature, the BiOBr@PMMA were obtained after centrifugation and washing with distilled water for several times, followed by freeze-drying at −40 °C under vacuum for 12 h.

Preparation of BiOBr@PILs

Briefly, 1.4 mmol of $Bi(NO_3)_3 \cdot 5H_2O$, 1.4 mmol of KBr, 0.02 g of PVP and 0.1 g of PILs were added slowly into 30 mL of ethylene glycol. The mixture was ultrasonically treated for 1 h, and then magnetically stirred for 2h. Subsequently, the mixture was transferred into a 50 mL Teflon-lined stainless steel autoclave. The autoclave was then sealed and maintained at 150 °C for 12 h. After cooling down to room temperature, the BiOBr@PILs were obtained after centrifugation and washing with distilled water for several times, followed by freeze-drying at −40 °C under vacuum for 12 h.

Evaluation of the mass transfer properties inside the ILG-microspheres

The mass transfer properties inside the ILG-microspheres were evaluated by immersing the ILG-microspheres into RhB aqueous solution, n-octane solution of coumarin 6, and fluorescein sodium aqueous solution, respectively, for 30 minutes under stirring, followed by 3 times of elution, and the isolated ILG-microspheres were then characterized by CLSM. The three fluorescent dyes selected here are all soluble in $[BMIM]PF_6$, while RhB, coumarin 6, and fluorescein sodium are positively charged, uncharged, and negatively charged, respectively.

Extraction of RhB by ILG-microspheres

Typically, extraction process was performed at room temperature (25 °C) as following: 0.1 g of ILG-microspheres was added into 10 mL aliquots of RhB aqueous solution with a concentration of 10 mg/L. After stirring the solution for a period of time, the supernatant was obtained by centrifuging (15,000 rpm for 10 min) for analysis with a PerkinElmer Lambda 35 UV-vis spectrometer.

Extraction-elution cyclic process of ILG-microspheres

0.1 g of ILG-microspheres was added into 10 mL of RhB aqueous solution (10 mg/L) with pH=2 under kept stirring to achieve extraction-adsorption equilibrium, and then the supernatant was obtained by centrifuging for analysis. Subsequently, the above-mentioned ILG-microspheres were continuously stirred in 10 mL of water with pH=11, and then the elution efficiency was tested with UV-vis spectrometer after reaching the elution equilibrium. Subsequently, after eluting the residual RhB in the ILG-microspheres, repeated the above operation steps for cyclic experiment.

Calculation of band gap energy (E_g) values for BiOBr-based catalysts

The band gap energy (E_g) values can be calculated by the Kubelka–Munk function (1) as follows:[1]

$$\alpha h\nu = A\left(h\nu - E_g\right)^{n/2} \tag{1}$$

where α is the optical absorption coefficient, $h\nu$ is the photonic energy, E_g is the band gap energy and A is a proportionality constant. Among them, n depends on the characteristics of the transition in a semiconductor, the BiOBr-based catalyst is an indirect semiconductor, so the parameter n is 4.[2]

Photodegradation of organic compounds by BiOBr-based catalysts

1. Photodegradation of RhB by BiOBr-based catalysts in static system

In a typical method, 0.05 g of photocatalyst was added into 100 mL of RhB aqueous solution with a concentration of 25 mg/L in a reaction beaker, and the reaction temperature was kept at 25 °C. Prior to irradiation, the suspensions were magnetically stirred in the dark for 10 min to achieve the adsorption equilibrium of the RhB on the catalyst. A 500 W Xenon lamp was used as the light source with the light intensity of 100 $\mathrm{mW{\cdot}cm^{-2}}$. Afterwards, illumination was performed, and 3 mL of the suspension was collected every minute and centrifuged (15,000 rpm for 10 min) to obtain the clarified solution for analysis with a PerkinElmer Lambda 35 UV-vis spectrometer.

2. Photodegradation kinetics of RhB by BiOBr-based catalysts

Furthermore, we fitted the experimental data of RhB degradation according to pseudo-first-order kinetic model to investigate the photocatalytic reaction kinetics. The pseudo-first-order kinetic model is expressed by equation (2), which is generally used for photocatalytic reactions of organic pollutants degradation:

$$\ln(C_0/C_t) = kt \tag{2}$$

where C_0 is the initial concentration of RhB before irradiation, C_t is the concentration of RhB in solution after certain time of irradiation, t is the irradiation time and k is the kinetic rate constant.

3. Photodegradation of ciprofloxacin by ILG-microspheres based liquid compartment microreactors in continuous-flow system

In a typical method, the photocatalytic membrane was laid in the sand core funnel (5 cm diameter) with valve, and then soaked with distilled water. The ciprofloxacin aqueous solution with a concentration of 30 mg/L was added dropwise to the funnel by peristaltic pump under the irradiation of a 500 W Xenon lamp. The flow rate was kept as 0.6 mL/min by adjusting the peristaltic pump and valve, and a sample was collected every 3 minutes. Finally, the concentration of ciprofloxacin in the effluent was analyzed by UV-vis spectrometer.

Theoretical simulation of concentration fields of RhB on BiOBr@ILG-microspheres during photocatalytic process

Theoretical simulation of concentration fields of RhB on BiOBr@ILG-microspheres were performed on COMSOL Multiphysics software. The theoretical section, including the formulation of the entire rates of adsorption and catalysis on BiOBr@ILG-microspheres along with systematic and step-by-step approaches for the diffusional model, is described as follows.[3, 4]

In the dark state adsorption process:

The concentration distribution of each component inside the BiOBr@ILG-microspheres is calculated by Fick's law Eq. (3):

$$\frac{\partial c}{\partial t} = - D_i\left(\frac{1}{r}\frac{\partial}{\partial r}\left(r\frac{\partial c}{\partial r}\right) + \frac{\partial^2 c}{\partial Z^2}\right) + E \tag{3}$$

where E, c, t, r, Z and D_i are the adsorption rate of RhB, the concentration of RhB, the reaction time, radius of sample, spatial direction, and the diffusivity coefficient of RhB, respectively.

Here, E is introduced according to the equation (4), and can be calculated by Langmuir adsorption isothermal model (5) and kinetic adsorption model (6):

$$E = - \frac{dc}{dt} = k_e c \tag{4}$$

$$q_e = \frac{q_{max} K_L c_e}{1 + K_L c_e} \tag{5}$$

$$\ln\left(q_e - q_t\right) = \ln\left(q_e\right) - k_e t \tag{6}$$

where k_e, q_e, q_{max}, c_e and K_L are the adsorption reaction rate constant, adsorption capacity at adsorption equilibrium, the maximum adsorption capacity, concentration at adsorption equilibrium, and constant of Langmuir, respectively.

In the photodegradation process:

The concentration distribution of each component inside the BiOBr@ILG-microspheres is calculated by Fick's law Eq. (7):

$$\frac{\partial c}{\partial t} = - D_i\left(\frac{1}{r}\frac{\partial}{\partial r}\left(r\frac{\partial c}{\partial r}\right) + \frac{\partial^2 c}{\partial Z^2}\right) + R \tag{7}$$

where R, c, t, r, Z and D_i are the degradation rate of RhB, the concentration of RhB, the reaction time, radius of sample, spatial direction, and the diffusivity coefficient of RhB, respectively.

Here, R is introduced according to the equation (8), and can be calculated by the pseudo-first-order kinetic model (9):

$$R = -\frac{dc}{dt} = k_r c \tag{8}$$

$$\ln\left(\frac{c_t}{c_0}\right) = -k_r t \tag{9}$$

where k_r, c_t, c_0 are catalytic kinetic rate constant, the concentration of RhB after catalytic degradation for a certain time, and the initial concentration of RhB, respectively.

The boundary conditions:

The interface between BiOBr and solution followed the adsorption equation (10) during the dark state adsorption process, and followed the adsorption equation (10) and catalytic equation (11) at the same time during the photodegradation process.

$$c_{t1} = c_{max(BiOBr)} * \left(1 - e^{-k_{e(BiOBr)} t_1}\right) \tag{10}$$

$$c_{t2} = c_{max(BiOBr)} * e^{-k_r t_2} \tag{11}$$

The interface between ILG-microspheres and solution only followed the adsorption equation (12) during the dark state adsorption process and the photodegradation process.

$$c_{t1} = c_{max(IL-microgels)} * \left(1 - e^{-k_{e(IL-microgels)} t_1}\right) \tag{12}$$

The interface between BiOBr and ILG-microspheres followed the catalytic equation (13) during the photodegradation process.

$$c_{t2} = c_{max(IL-microgels)} * e^{-k_r t_2} \tag{13}$$

where $c_{max(BiOBr)}$, $c_{max(ILG\text{-}microspheres)}$, $k_{e(BiOBr)}$, $k_{e(ILG\text{-}microspheres)}$, t_1, t_2 and k_r are the maximum adsorption capacity of RhB by BiOBr, the maximum adsorption capacity of RhB by ILG-microspheres, the adsorption reaction rate constant of BiOBr, the adsorption reaction rate constant of ILG-microspheres, adsorption time, catalytic time, and catalytic kinetic rate constant of BiOBr@ILG-microspheres.

Characterization and instruments

FTIR was performed on a Thermo Nicolet NEXUS-470 (USA) spectrometer using potassium bromide pellet technique. UV-vis was performed on a PerkinElmer Lambda 35 (USA) spectrometer using distilled water as solvent. UV-visible diffuse reflectance spectroscopy (DRS) was performed on a RF-5301PC spectrometer (SHIMADZU, Japan) using barium sulfate tablets as a reference. NMR measurements included solid state nuclear magnetic resonance (SSNMR) and liquid state nuclear magnetic resonance (LSNMR). SSNMR was tested at room temperature on a 400 MHz spectrometer (Bruker BioSpin GmbH, Germany), tetramethylsilane (TMS) as external chemical shift reference. LSNMR was tested on a Mercury Vx-300 MHz spectrometer (Varian, USA), $CDCl_3$ as solvent and TMS as internal standard. XRD was performed on a D8-Advance X-ray powder diffractometer (Bruker, Germany) with Cu Kα radiation (λ=1.54051 Å), the 2θ was from 5° to 80°. TGA and DSC were performed on a Q600 integrated thermal analyzer (Waters Corporation, USA) with a heating rate of 5 °C/min in nitrogen atmosphere, and the weights of samples were approximately 10 mg. SEM measurements were performed on a Hitachi SU-8010 (JEOL, Japan) electron microscope at an acceleration voltage of 10 kV. EDS was conducted utilizing electron microscope equipped with XFlash Detector 5030 (Bruker, Germany). TEM measurements were performed on a Hitachi JEM-2100 (JEOL, Japan) electron microscope with an acceleration voltage of 200 kV. AFM measurements were performed on Bruker Dimension Icon (Germany) with NanoScope. N_2 adsorption/desorption isotherms were measured on an ASAP 2460 (Micromeritics, USA) at 77 K. Static contact angle (SCA) was measured by dropping deionized water on the surface of pressed sample at room temperature and analyzed with an SDA-100 instrument (Kruss, Germany). Confocal micrographs were taken with a TCS-SP8 (Leica, Germany) confocal laser scanning microscope (CLSM), the excitation wavelengths of RhB, coumarin 6 and fluorescein sodium were 555, 360, and 524 nm, respectively. XPS was conducted via an Axis Ultra DLD (Kratos, UK) spectrometer with an Al Kα radiation under ultrahigh vacuum condition. The photocurrent density-time (I-t) curves were tested by electrochemistry workgroup (CHI660E, Shanghai) in a two-electrode system including the anode was FTO glass sheet (1.5 cm×1.5 cm) coated with 0.03g sample, the cathode was a platinum wire, the electrolyte was 0.5 M Na_2SO_4 aqueous solution, and a 500 W Xenon lamp was used as the light source with a power density of 100 $mW\cdot cm^{-2}$. The surface photovoltage measurement system is made up of a 500 W Xenon lamp, a lock-in amplifier (SR830-DSP) with a light chopper (SR540), a sample cell and a computer.[5] In the photovoltaic cell the FTO glass sheet with samples acted as a bottom electrode, a platinum wire gauze was used for top electrode and a spacer of mica was inserted between the two electrodes, and with lock-in amplifier we can obtain surface photovoltage amplitude. The transient photovoltage measurement were performed in air atmosphere at indoor temperature, a 355 nm laser pulse of 10 ns width was used to excite the samples, and the photovoltaic signal was recorded in the range from 10 ns to 10 ms. GC-MS system (Ultra GC Polaris Q, Thermo, USA) with the SH-Rxi-5Sil column (30.0 m×0.25 mm×0.25 μm), and the oven temperature was started at 50 °C (2 min hold), then increased to 300 °C at a ramp rate of 10 °C /min and held for 10 min. The stability of the emulsions were measured using a Turbiscan Lab Expert analyzer (Formulaction Inc., Toulouse, France). The emulsions were placed in an instrument- specific test glass bottle and scanned every 30 min continuously for 24 h. The stability of the emulsions was determined by the Turbiscan stability index (TSI) using the Turbiscan software.

Supplementary Figures

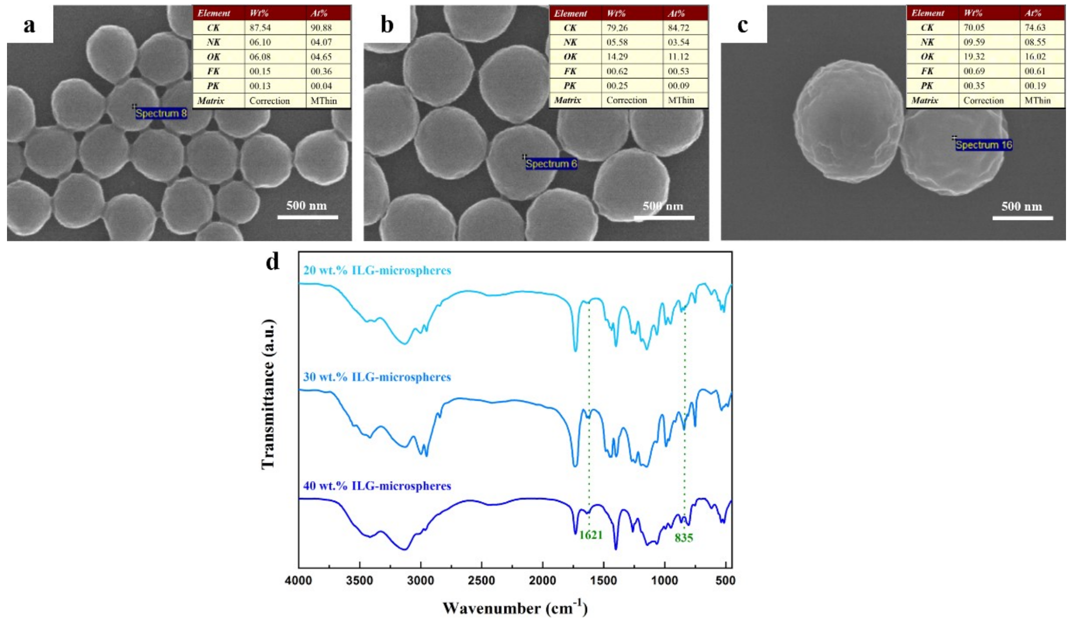

Element	*Wt%*	*At%*
CK	87.54	90.88
NK	06.10	04.07
OK	06.08	04.65
FK	00.15	00.36
PK	00.13	00.04
Matrix	Correction	MThin

Element	*Wt%*	*At%*
CK	79.26	84.72
NK	05.58	03.54
OK	14.29	11.12
FK	00.62	00.53
PK	00.25	00.09
Matrix	Correction	MThin

Element	*Wt%*	*At%*
CK	70.05	74.63
NK	09.59	08.55
OK	19.32	16.02
FK	00.69	00.61
PK	00.35	00.19
Matrix	Correction	MThin

Fig. S1. SEM and EDS images of the eluted ILG-microspheres. (a) 20 wt.% ILG-microspheres; (b) 30 wt.% ILG-microspheres; (c) 40 wt.% ILG-microspheres; (d) FTIR spectra of the eluted ILG-microspheres.

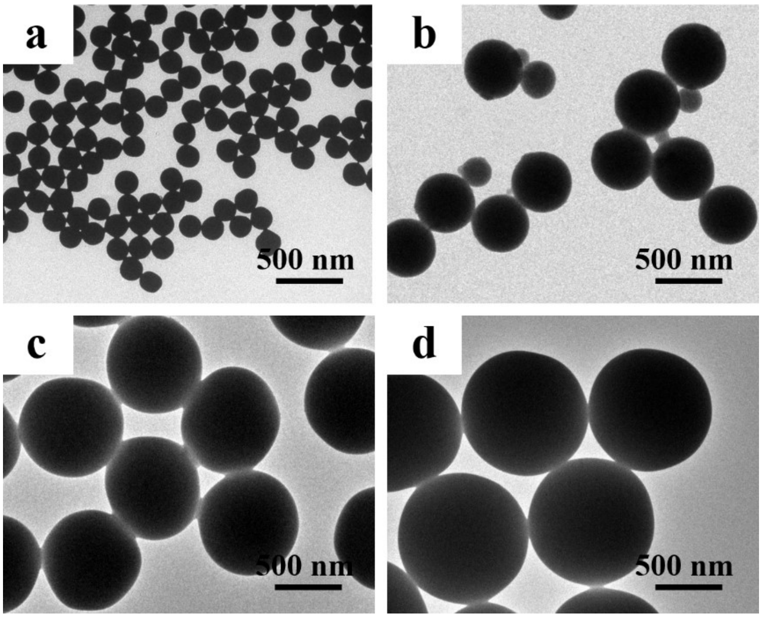

Fig. S2. TEM images of ILG-microspheres with different ILs contents (a) 0 wt.%, (b) 20 wt.%, (c) 30 wt.%, (d) 40 wt.%.

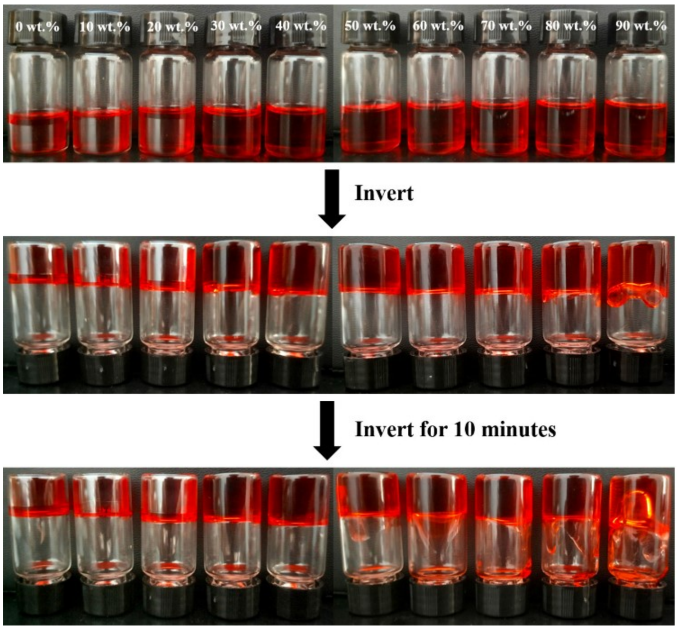

Fig. S3. The photographs of bulk IL-gels (the gel network is PMMA and the dispersive medium is [BMIM]PF$_6$) dyed by Sudan III.

It can be seen from the photographs that the Pickering emulsions stabilized by pure PMMA microspheres are W/O type, and the diameters of droplets are in the range of 200–400 μm. The Pickering emulsions stabilized by ILG-microspheres are O/W type, and the average diameters of droplets are ca. 700 μm. The Turbiscan stability index (TSI) was tested to investigate the stability of emulsions, and the high TSI value indicates low stability of the emulsions. As shown in Fig. S4e, the 0 wt.% ILG-microspheres (PMMA microspheres) has the highest TSI value and the fastest growth rate, indicating that the stability of W/O Pickering emulsions stabilized by PMMA microspheres is poorer than the O/W Pickering emulsions stabilized by ILG-microspheres. In addition, the low TSI value of the emulsions stabilized by 30 wt.% ILG-microspheres indicates that the relatively stable emulsion droplets were formed. This result is consistent with the relatively uniform emulsion droplets formed by 30 wt.% ILG-microspheres in Fig. S4c.

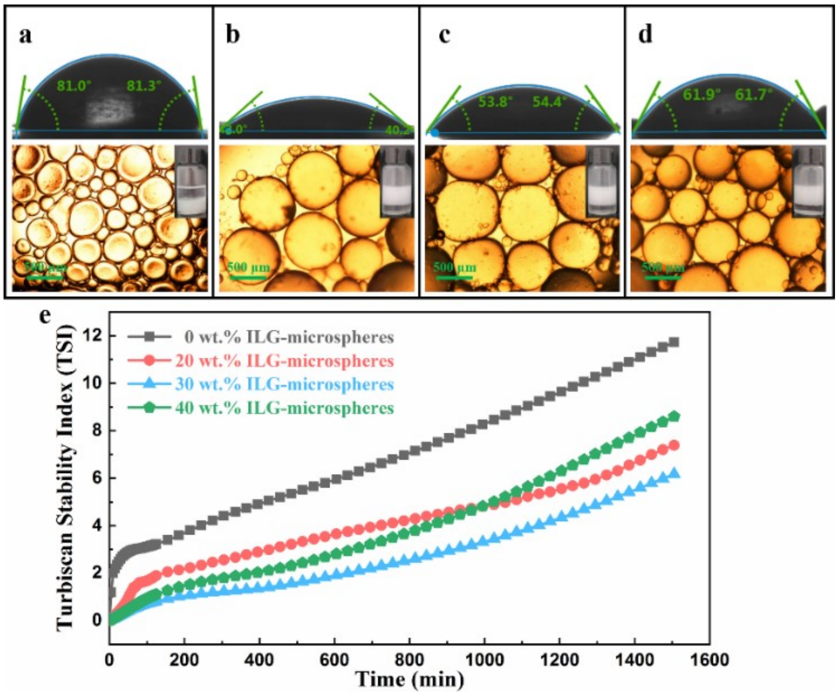

Fig. S4. The static water contact angles of ILG-microspheres; photographs and optical microscopic images of Pickering emulsions stabilized by ILG-microspheres (500 nm) with different mass percentages of [BMIM]PF_6 after standing for 7 days at room temperature. (a) 0 wt.%; (b) 20 wt.%; (c) 30 wt.%; (d) 40 wt.%. (e) TSI values of Pickering emulsions stabilized by ILG-microspheres. (The Pickering emulsions was prepared by 0.02 g ILG-microspheres, 3 mL deionized water, and 3 mL n-octane)

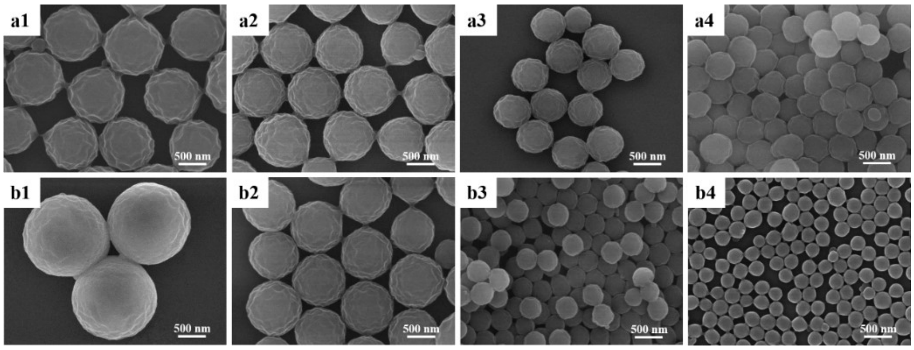

Fig. S5. SEM images of ILG-microspheres prepared under the different reaction conditions. (a) different volumes of water: (a1) 60 mL, (a2) 80 mL, (a3) 100 mL, (a4) 120 mL; (b) different addition concentrations of PVP: (b1) 0.5 g/L, (b2) 1 g/L, (b3) 2 g/L, (b4) 4 g/L.

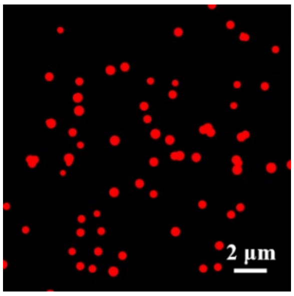

Fig. S6. The CLSM images of ILG-microspheres.

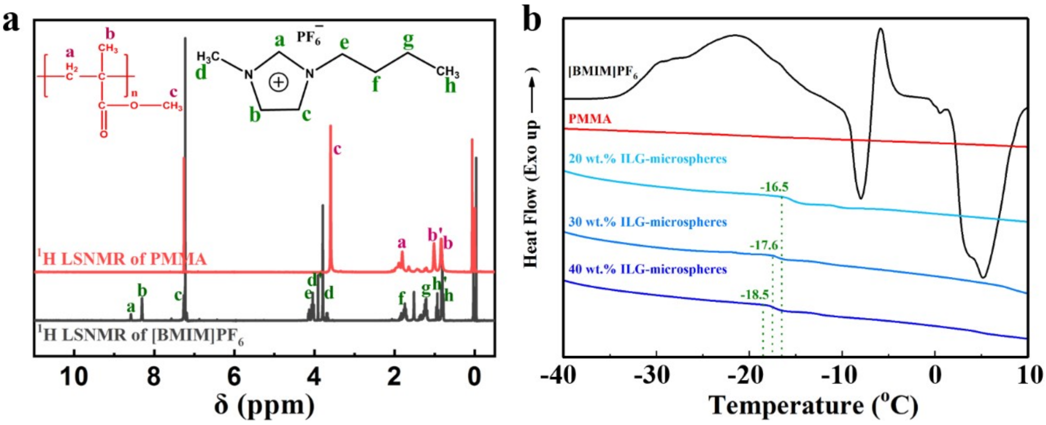

Fig. S7. (a) ^{1}H NMR spectra of [BMIM]PF$_6$ and PMMA; (b) DSC curves of [BMIM]PF$_6$, PMMA and ILG-microspheres.

It can be seen from the Fig. S8 that PMMA has more and larger light spots under the polarizing microscope, and the light spots gradually become less and smaller with the increase of ILs content in ILG-microspheres. It shows that [BMIM]PF$_6$ can reduce the crystallinity of the PMMA networks, increase the mobility of molecular chains in amorphous region, and then increase its free volume.

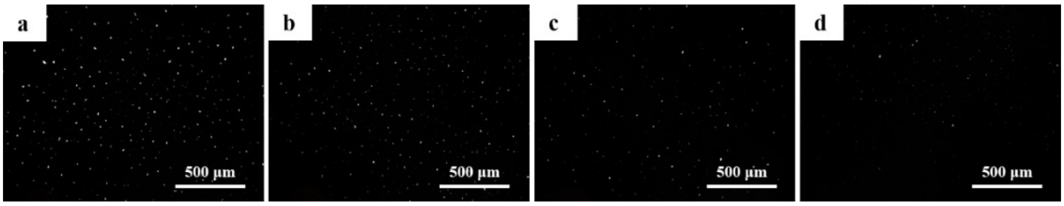

Fig. S8. Polarized optical microscope images of the ILG-microspheres after hot pressing film forming method. (a) 0 wt.% ILG-microspheres; (b) 20 wt.% ILG-microspheres; (c) 30 wt.% ILG-microspheres; (d) 40 wt.% ILG-microspheres.

As shown in Fig. S9a, the extraction efficiency of RhB by the ILG-microspheres is about 100% under the condition of pH=2, and the elution efficiency is about 65% when the pH=11. As shown in Fig. S9b, after 5 cycles of extraction-elution experiments, the extraction efficiency (pH=2) and elution efficiency (pH=11) of RhB by ILG-microspheres decreased from 100% and 65% to 92% and 55%, respectively.

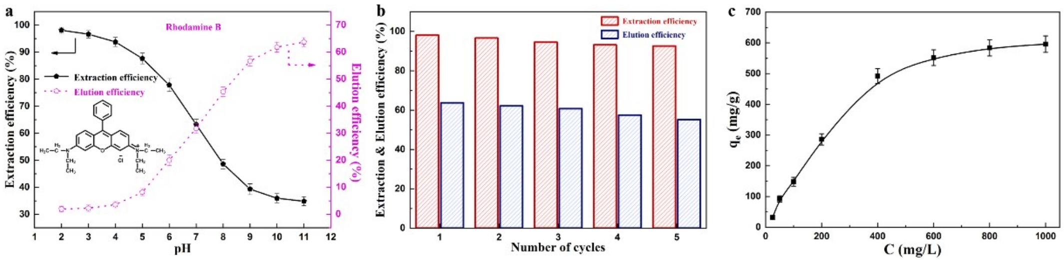

Fig. S9. (a) The effect of solution pH on extraction-elution efficiency of ILG-microspheres (30 wt.%, 500 nm) towards RhB; (b) cyclic experiments on extraction-elution of RhB by ILG-microspheres (30 wt.%, 500 nm); (c) adsorption isothermal curves for extraction-adsorption of RhB by ILG-microspheres (30 wt.%, 500 nm) at pH=7.

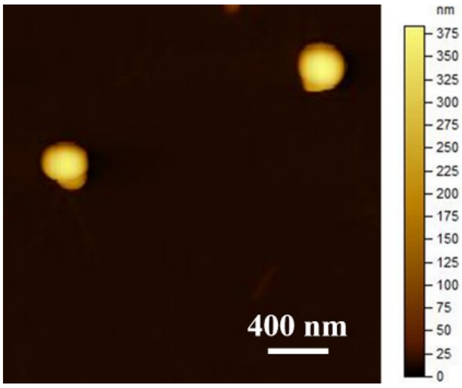

Fig. S10. AFM images of ILG-microspheres (40 wt.%, 300 nm)

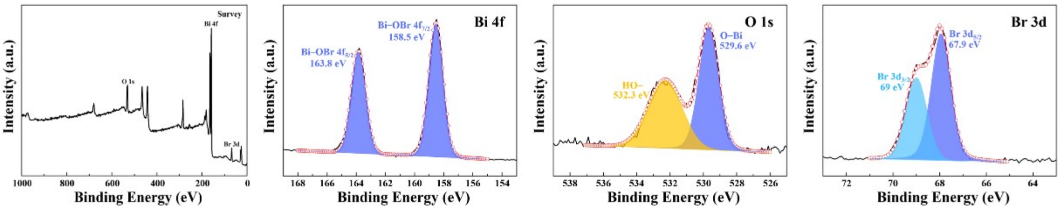

Fig. S11. The XPS spectra of BiOBr.

The surface photovoltage spectra result for pure BiOBr microspheres and BiOBr@ILG-microspheres are shown in Fig. S12a. The surface photovoltage signal of the BiOBr@ILG-microspheres is positive under illumination wavelength of 300–600 nm, and the maximum value is 0.067 mV at 336 nm. The surface photovoltage signal of the pure BiOBr is positive under illumination wavelength of 300–415 nm, while negative (below 0 V) under illumination wavelength of 415–600 nm, respectively. Therefore, under the irradiation of simulated sunlight, different excitation wavelengths will cause different separation directions of photogenerated charges on the pure BiOBr, which increases the probability of charge recombination, resulting in its catalytic activity lower than that of BiOBr@ILG-microspheres. To further study the semiconductor conductivity type and charge transfer kinetics, we carried out the transient photovoltage measurements of samples. As shown in Fig. S12b, the positive transient photovoltage responses of pure BiOBr microspheres and BiOBr@ILG-microspheres give direct evidence of n-type conductivity. In addition, there are two kinds of separation models for photogenerated charges transfer in photocatalyst: drift under built-in electric field and diffusion under concentration gradient. In general, the drift process usually generated a fast transient photovoltage response at short timescale.[6, 7] Therefore, the drift processes of pure BiOBr and BiOBr@ILG-microspheres reached the highest value at the level of 3×10^{-7} s. However, the photogenerated charges produced by BiOBr@ILG-microspheres have a longer transfer time during the diffusion process than that of pure BiOBr, indicating that the photogenerated charges produced by BiOBr@ILG-microspheres have a longer lifetime and BiOBr@ILG-microspheres possess longer catalytic activity.[8]

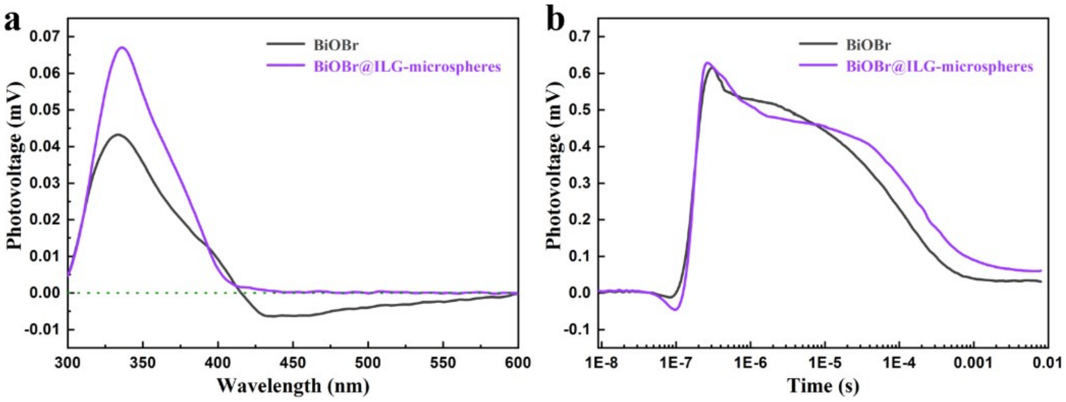

Fig. S12. (a) The field-induced surface photovoltage spectroscopies of pure BiOBr microspheres and BiOBr@ILG-microspheres; (b) the transient photovoltage responses of pure BiOBr microspheres and BiOBr@ILG-microspheres excited by 355 nm laser pulse.

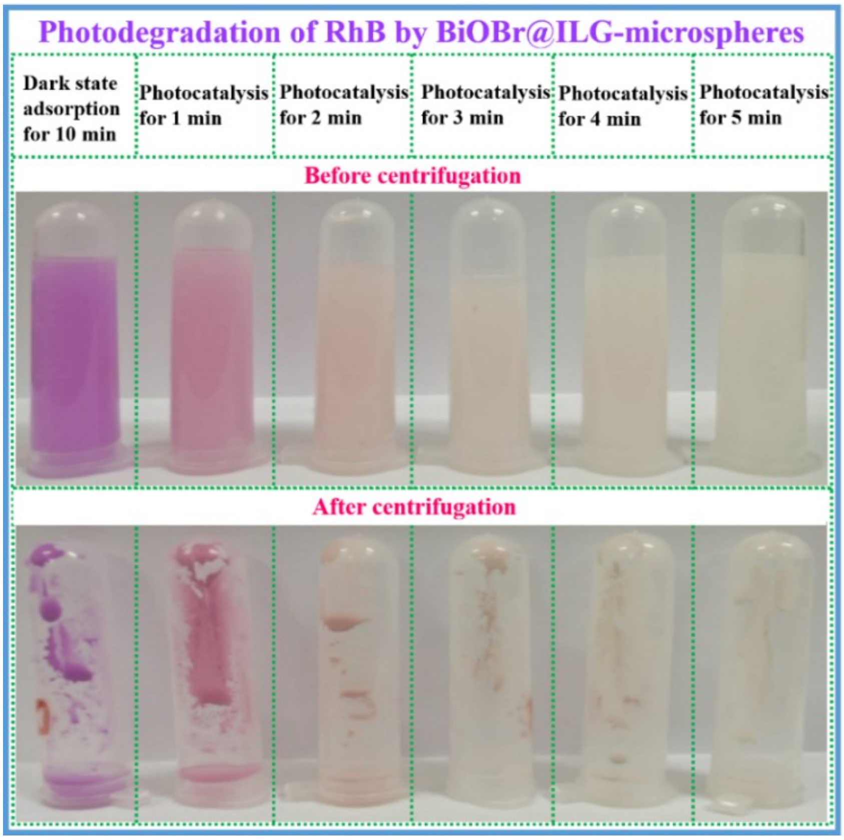

Fig. S13. The photographs of adsorption and photodegradation of RhB by BiOBr@ILG-microspheres.

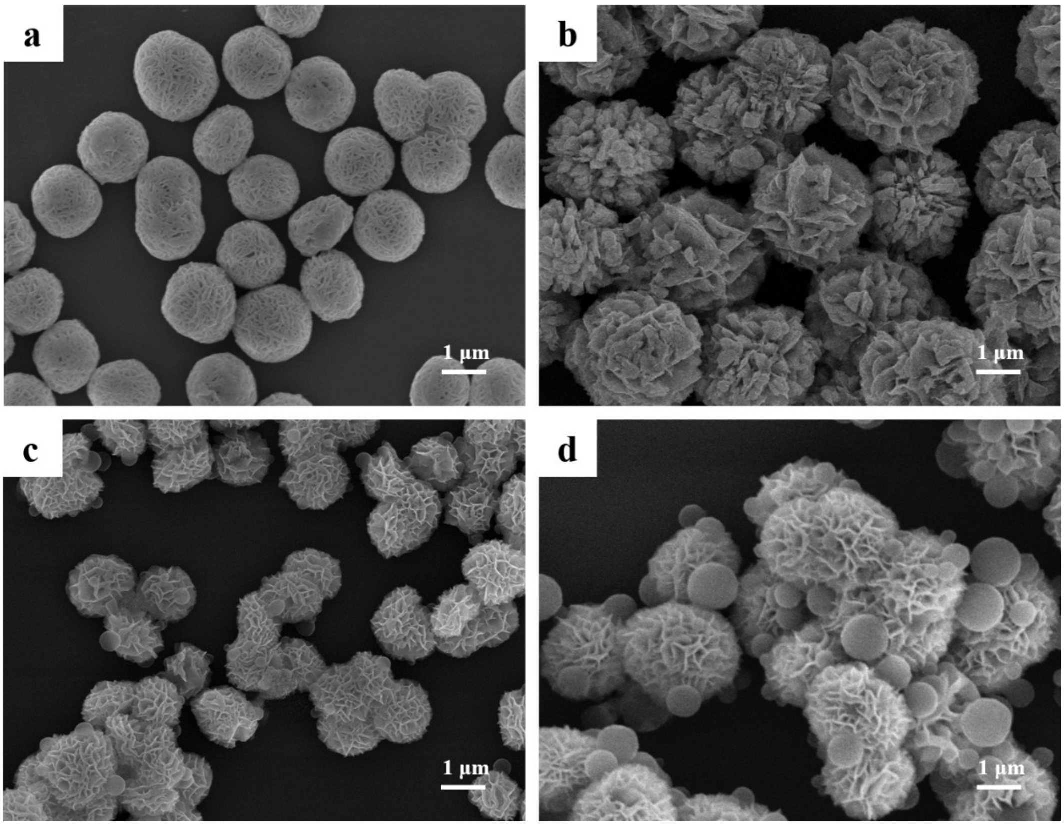

Fig. S14. SEM of samples. (a) BiOBr microspheres; (b) BiOBr-[BMIM]PF_6; (c) BiOBr@PMMA; (d) BiOBr@PILs.

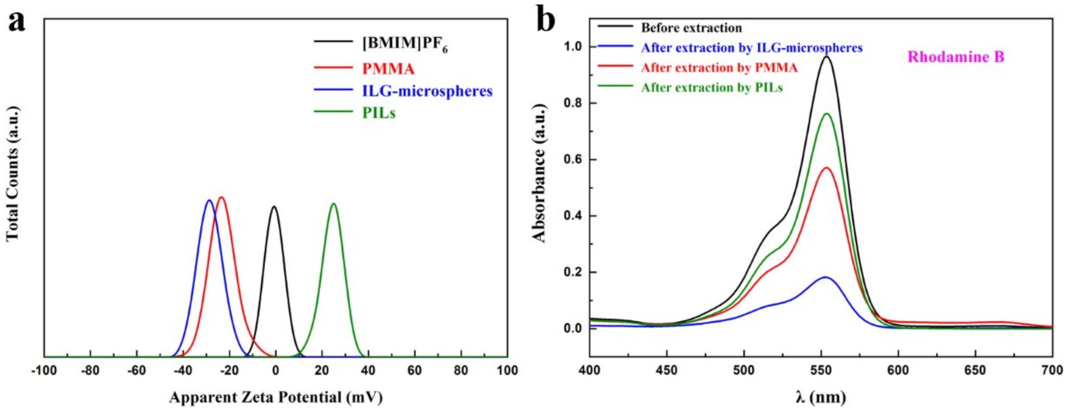

Fig. S15. (a) The Zeta potentials of [BMIM]PF_6, PMMA, ILG-microspheres (40 wt.%, 300 nm) and PILs; (b) UV-vis spectra of RhB aqueous solution after extraction by 0.1 g of PMMA, ILG-microspheres (40 wt.%, 300 nm) and PILs, respectively.

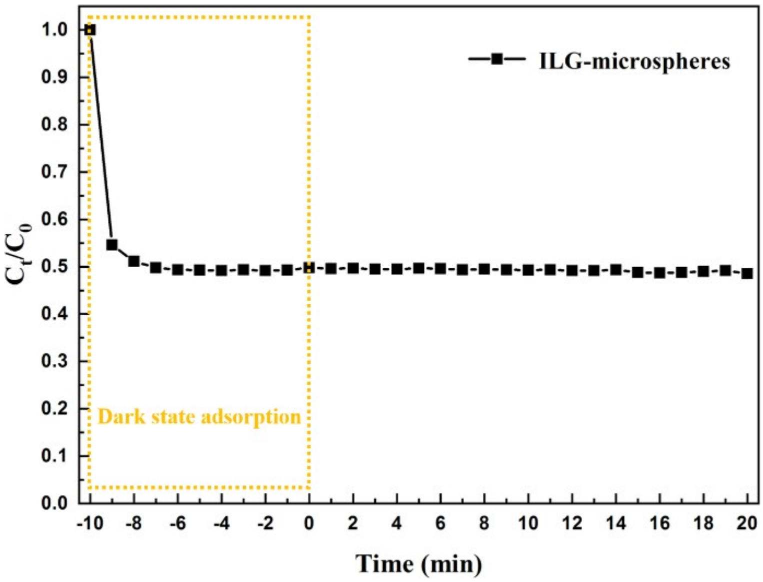

Fig. S16. The photodegradation efficiency of RhB by 0.05 g of ILG-microspheres (40 wt.%, 300 nm).

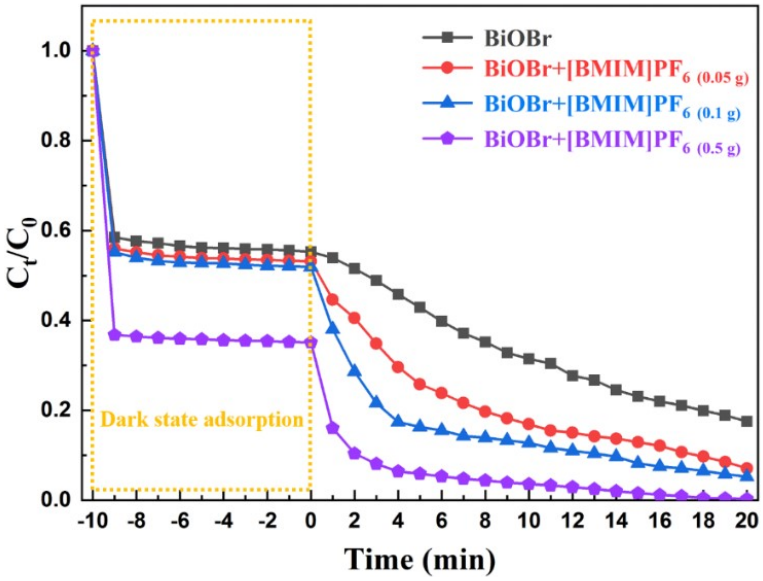

Fig. S17. The effect of content of the mixed ILs on photodegradation efficiency of RhB by BiOBr.

As shown in Figs. S18b and S18c, the morphology and structure of the BiOBr@ILG-microspheres have not been destroyed and the ILG-microspheres do not fall off from the BiOBr, indicating that the BiOBr@ILG-microspheres have good structural stability. In addition, the small particles on the surface of ILG-microspheres in BiOBr@ILG-microsphere may be BiF_3 formed by the reaction of $[BMIM]PF_6$ with $Bi(NO_3)_3{\cdot}5H_2O$.

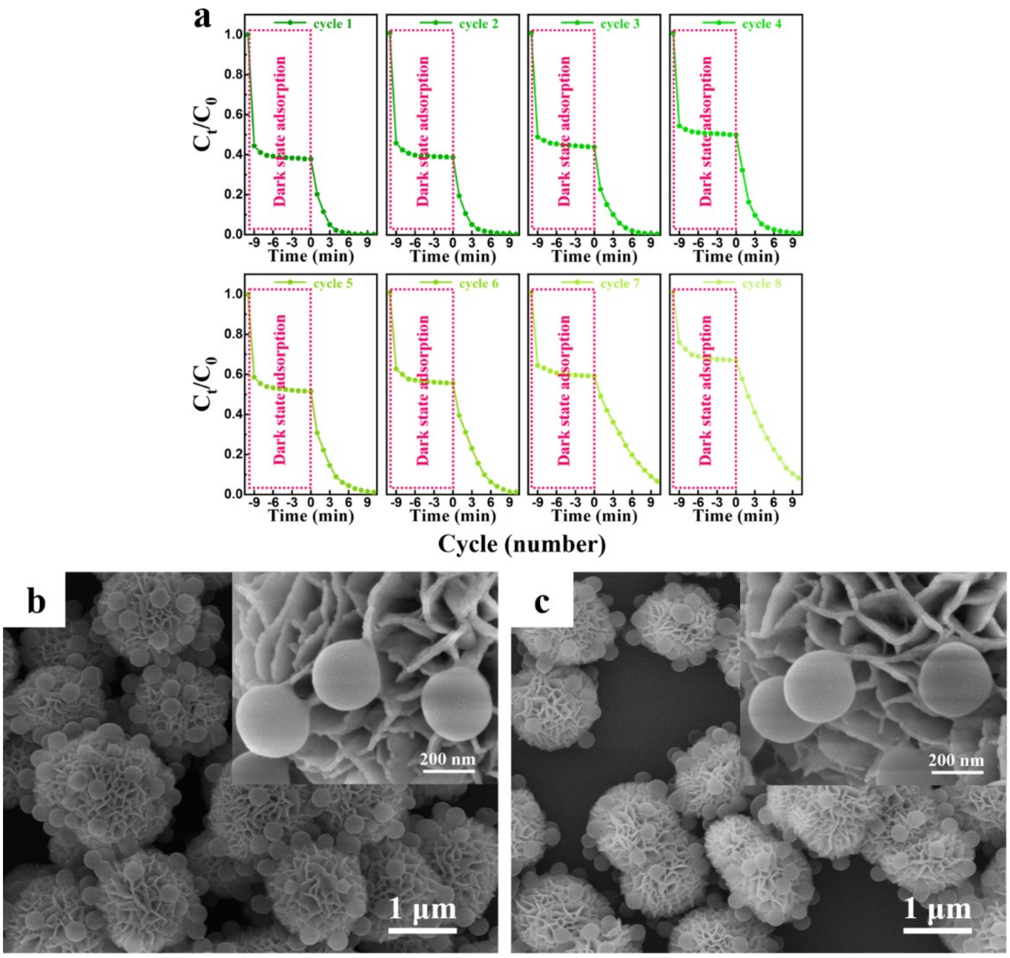

Fig. S18. (a) Cyclic experiments of photodegradation of RhB by BiOBr@ILG-microspheres; (b) SEM of original BiOBr@ILG-microspheres; (c) SEM of BiOBr@ILG-microspheres after 8 times cycling.

According to the analysis of intermediates by GC-MS (Fig. S19c), the probable pathway of ciprofloxacin degradation is proposed as presented in Fig. S19b. In this regard, we assumed that the piperazine ring was firstly opened by attack of the ·OH and holes. Subsequently, the $\cdot O_2^-$, ·OH and the holes attacked in proper sequence the derivatives of piperazine ring, and then low molecular weight intermediates were obtained by a series of reactions such as dealcoholization, dealkylation, decarboxylation, defluorination, and ring-opening reaction.[9, 10] Finally, the intermediates were completely degraded into H_2O, CO_2 and some inorganic ions by mineralization.

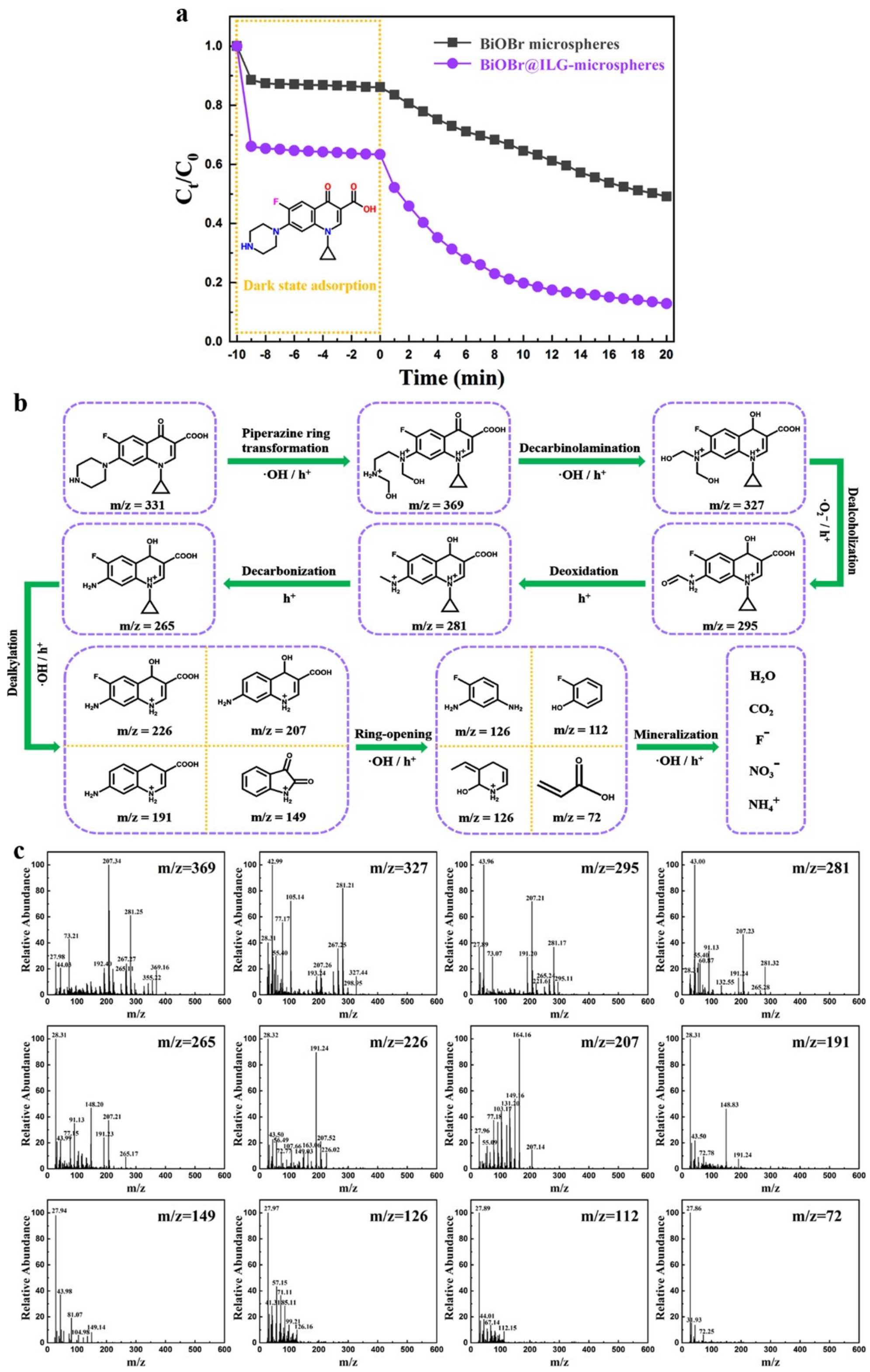

Fig. S19. (a) Photodegradation efficiencies of ciprofloxacin as a function of irradiation time; (b) possible photodegradation pathway of ciprofloxacin by BiOBr@ILG-microspheres under illumination; (c) MS spectra of photodegradation products.

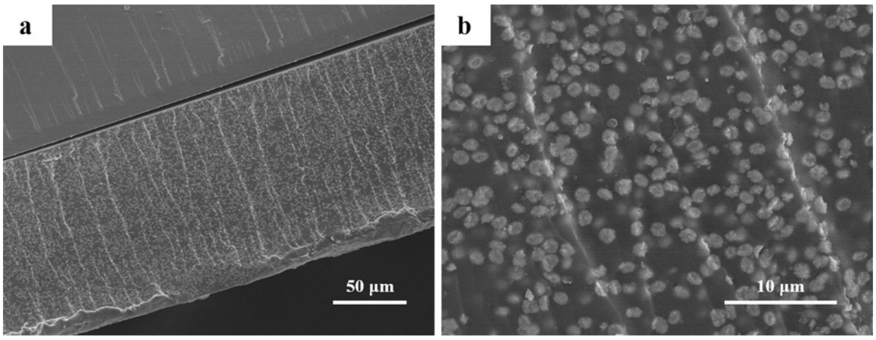

Fig. S20. SEM of the fracture-surface of the multi-liquid phase membrane under different magnification.

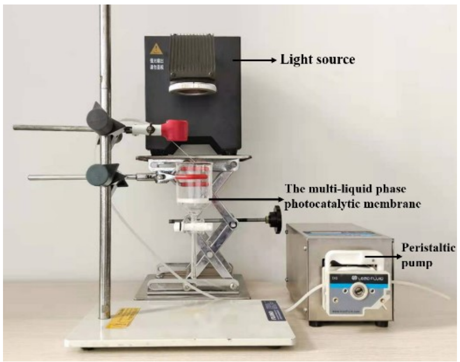

Fig. S21. The photograph of the flow photocatalytic device.

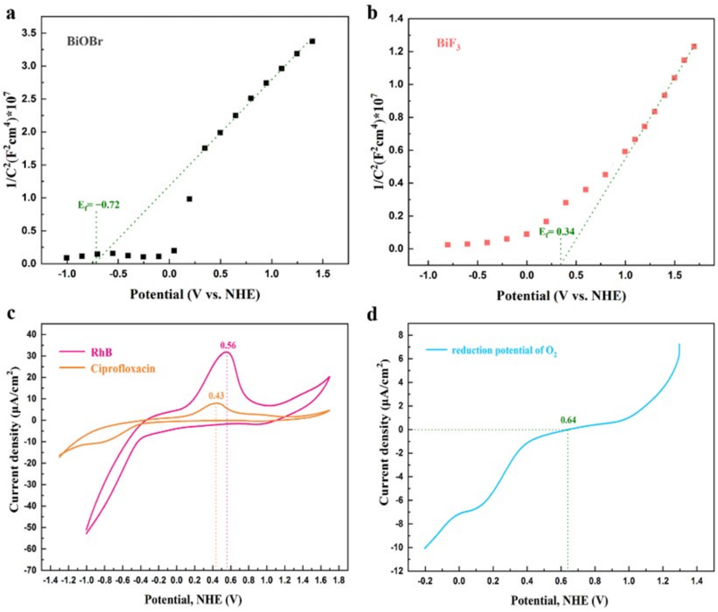

Fig. S22. Variation of capacitance with the applied potential in 0.5 M Na_2SO_4 presented in the Mott-Schottky relationship for BiOBr (a) and BiF_3 (b); (c) CV curves of the BiOBr@ILG-microspheres electrode in RhB (25 mg/L) and ciprofloxacin (30 mg/L) aqueous solution under illumination, respectively; (d) LSV curve of the BiOBr@ILG-microspheres electrode in 0.5 M Na_2SO_4 with oversaturated dissolved oxygen under illumination.

Supplementary Tables

Table S1.

Table S1. The mass percentage of $[BMIM]PF_6$ inside the ILG-microspheres

	20 wt.% ILG-microspheres	**30 wt.% ILG-microspheres**	**40 wt.% ILG-microspheres**
m_a	**0.1003 g**	**0.1007 g**	**0.1002 g**
m_b	**0.0788 g**	**0.0698 g**	**0.0616 g**
m_a-m_b	**0.0215 g**	**0.0309 g**	**0.0386 g**
$(m_a-m_b)/m_a$ %	**21.44 %**	**30.68 %**	**38.52 %**

Table S2.

Table S2. The ^{1}H chemical shifts of $[BMIM]PF_6$ and PMMA

Compound	**δ (ppm)**	**Assignment**
$[BMIM]PF_6$	**8.585, 8.306, 7.259**	**imidazole framework**
	4.053	**$–CH_2N$**
	3.926, 3.773	**$–CH_3N$**
	1.765, 1.205	**$–CH_2–$**
	0.922, 0.796	**$–CH_3$**
PMMA	**3.596**	**$–CH_3O$**
	1.815	**$–CH_2–$**
	0.999, 0.822	**$–CH_3C$**

Table S3.

Table S3. Comparisons of ILG-microspheres with other materials for adsorption of RhB (pH=7)

Materials	Maximal adsorption capacity	Equilibration time	Article information
Mixed hemi/ad-micelle SDS-coated magnetic iron oxide nanoparticles	385 mg/g	4 min	Anal. Chem. 2015, 87, 7894-7901 DOI: 10.1021/acs.analchem.5b01676
Silsesquioxane-based thiophene-bridged hybrid nanoporous network	1402 mg/g	90 min	J. Mater. Chem. A 2016, 4, 16714-16722 DOI: 10.1039/c6ta06656a
Hierarchical SnS_2	200 mg/g	25 min	J. Colloid Interface Sci. 2017, 507, 225-233 DOI: 10.1016/j.jcis.2017.07.053
Carbon nanospheres	63.85 mg/g	10 min	Appl. Surf. Sci. 2019, 484, 144-151 DOI: 10.1016/j.apsusc.2019.04.080
Reduced-graphene-oxide/rare-earth-metal-oxide Aerogels (RGO/REMO)	243.4 mg/g	1500 min	Appl. Surf. Sci. 2020, 504, 144377 DOI: 10.1016/j.apsusc.2019.144377
Activated carbon	123.46 mg/g	12 min	J. Cleaner Prod. 2020, 253, 119989 DOI: 10.1016/j.jclepro.2020.119989
Nitrogen-doped mesoporous carbons	204.08 mg/g	60 min	J. Hazard. Mater. 2020, 391, 122163 DOI: 10.1016/j.jhazmat.2020.122163
Magnetic montmorillonite composite γ-Fe2O3@Mt	209.2 mg/g	30 min	J. Mol. Liq. 2020, 309, 113142 DOI: 10.1016/j.molliq.2020.113142
Nitrogen self-doped biochar	839.97 mg/g	30 min	J. Cleaner Prod. 2022, 332, 130069 DOI: 10.1016/j.jclepro.2021.130069
ILG-microspheres	596 mg/g	7 min	This work

Table S4.

Table S4. The specific surface area, pore volume and pore diameter of BiOBr microspheres and BiOBr@ILG-microspheres

	Specific surface area	Pore volume	Pore diameter
BiOBr microspheres	44.172 m^2/g	0.092 cm^3/g	3.825 nm
BiOBr@ILG-microspheres	60.105 m^2/g	0.137 cm^3/g	7.592 nm

Table S5.

Table S5. Comparisons of BiOBr@ILG-microspheres with other BiOBr-based catalysts for photodegradation of RhB

Materials	Substrate	Adsorption capacity	Photocatalytic performance	Photo-source	Article information
BiOBr microspheres (25 mg)	RhB aqueous solution (50 mL, 20 mg/L)	$C/C_0 \approx 94$ % (60 min)	degradation rate: ~ 100 % (50 min)	500 W xenon lamp (600 mW·cm^{-2}, $\lambda > 420$ nm)	Appl. Catal. B: Environ. 2012, 111-112, 334-341 DOI: 10.1016/j.apcatb.2011.10.016
BiOBr lamellar (40 mg)	RhB aqueous solution (40 mL, 20 mg/L)	$C/C_0 = 33$ % (60 min)	degradation rate: ~ 100 % (30 min)	500 W xenon lamp ($\lambda \geq 400$ nm)	J. Mater. Chem. A 2013, 1, 8622-8629 DOI: 10.1039/c3ta11390f
BiOBr/montmorillonite composites (50 mg)	RhB aqueous solution (50 mL, 40 mg/L)	$C/C_0 = 29.62$ % (60 min)	degradation rate: 98.96 % (60 min)	1000 W xenon lamp ($\lambda > 420$ nm)	J. Hazard. Mater. 2014, 275, 185-192 DOI: 10.1016/j.jhazmat.2014.04.064
$BiOBr/Bi_{24}O_{31}Br_{10}$ heterojunctions (100 mg)	RhB aqueous solution (100 mL, 50 mg/L)	$C/C_0 = 85.3$ % (30 min)	degradation rate: ~ 100 % (40 min)	350 W xenon lamp (450 mW·cm^{-2}, $400 < \lambda < 1064$ nm)	Nanoscale 2015, 7, 1116-1126 DOI: 10.1039/C4NR05451B
BiOBr–titanium phosphate composites (20 mg)	RhB aqueous solution (50 mL, 5 mg/L)	adsorption quantity is 7.2 %	degradation rate: ~ 100 % (8 min)	300 W xenon lamp ($\lambda > 420$ nm)	Dalton Trans 2016, 45, 13907-13916 DOI: 10.1039/c6dt02582j
Ag_3VO_4/BiOBr heterojunctions (30 mg)	RhB aqueous solution (50 mL, 10 mg/L)	$C/C_0 \approx 92$ % (30 min)	degradation rate: 98.7 % (15 min)	300 W xenon lamp ($\lambda > 420$ nm)	Molecular Catalysis 2017, 436, 190-198 DOI: 10.1016/j.mcat.2017.04.004
BiF_3/BiOBr heterojunctions (200 mg)	RhB aqueous solution (200 mL, 20 mg/L)	stirred in the dark (30 min)	degradation rate: ~ 100 % (40 min)	300 W xenon lamp	J. Hazard. Mater. 2019, 367, 304-315 DOI: 10.1016/j.jhazmat.2018.12.060
C_{60}/BiOBr (50 mg)	RhB aqueous solution (50 mL, 10 mg/L)	$C/C_0 \approx 72$ % (20 min)	degradation rate: 91 % (10 min)	500 W xenon lamp with a 420 nm filter	Appl. Surf. Sci. 2021, 540, 148340 DOI: 10.1016/j.apsusc.2020.148340
BiOAc/BiOBr heterojunction composites (25 mg)	RhB aqueous solution (50 mL, 10 mg/L)	$C/C_0 \approx 39$ % (30 min)	degradation rate: 98 % (15 min)	Nine 5 W LED lights ($\lambda > 390$ nm)	Sep. Purif. Technol. 2021, 261, 118286 DOI: 10.1016/j.seppur.2020.118286
BiOBr@ILG-microspheres (50 mg)	RhB aqueous solution (100 mL, 25 mg/L)	$C/C_0 = 37.5$ % (10 min)	degradation rate: ~ 100 % (7 min)	500 W xenon lamp (100 mW·cm^{-2})	This work

Supplementary Video

Video S1.

Video S1. The changes of wrinkles on the ILG-microspheres surface under electron beam stimulation

As shown in the Video S1, due to the stimuli-responsiveness of the ILG-microspheres, the more obvious wrinkles gradually appeared on the surface under the stimulation of electron beams.

References

[1] Y. Yang, F. Teng, Y. Kan, L. Yang, Z. Liu, W. Gu, A. Zhang, W. Hao and Y. Teng, Appl. Catal., B. 2017, 205, 412–420.

[2] X. Shi, X. Chen, X. Chen, S. Zhou, S. Lou, Y. Wang and L. Yuan, Chem. Eng. J. 2013, 222, 120-127.

[3] M. Hasanpour, S. Motahari, D. Jing and M. Hatami, Top. Catal. 2021. https://doi.org/10.1007/s11244-021-01451-y.

[4] W. Li, J. Chen, S. Zhao, T. Huang, H. Ying, C. Trujillo, G. Molinaro, Z. Zhou, T. Jiang, W. Liu, L. Li, Y. Bai, P. Quan, Y. Ding, J. Hirvonen, G. Yin, H.A. Santos, J. Fan and D. Liu, Nat. Commun. 2022, 13, 1262.

[5] Y. Zhang, D. Wang, S. Pang, Y. Lin, T. Jiang and T. Xie, Appl. Surf. Sci. 2010, 256, 7217-7221.

[6] Y. Zhang, S. Lin, W. Zhang, Y. Zhang, F. Qi, S. Wu, Q. Pei, T. Feng and X.-M. Song, Electrochim. Acta. 2014, 150, 167-172.

[7] Y. Wang, Y. Lan, D. Bu, B. Qian, Y. Wang, B. Wang, Q. Wu, S. Li, Y. Zhang and X.-M. Song, Electrochim. Acta. 2020, 352, 136476.

[8] J. Sun, X. Li, Q. Zhao and B. Liu, Appl. Catal., B. 2021, 281, 119478.

[9] X. Hu, X. Hu, Q. Peng, L. Zhou, X. Tan, L. Jiang, C. Tang, H. Wang, S. Liu, Y. Wang and Z. Ning, Chem. Eng. J. 2020, 380, 122366.

[10] Z. Jia, T. Li, Z. Zheng, J. Zhang, J. Liu, R. Li, Y. Wang, X. Zhang, Y. Wang and C. Fan, Chem. Eng. J. 2020, 380, 122422.